Computation

CrossMark

Structure and chemistry of liquid Al–Cu alloys: molecular dynamics study versus thermodynamics-based modelling

Marcela E. Trybula[1,2,*] (iD), Przemysław W. Szafrański[3], and Pavel A. Korzhavyi[2]

[1] *Institute of Metallurgy and Materials Science Polish Academy of Sciences, 30-059 Kraków, Poland*
[2] *Department of Materials Science and Engineering, KTH Royal Institute of Technology, 100-44 Stockholm, Sweden*
[3] *Jagiellonian University Medical College, 30-688 Kraków, Poland*

ABSTRACT

Classical molecular dynamics simulations, employing a modified embedded atom model (MEAM) parametrization recently developed by Trybula, have been performed and combined with thermodynamics-based modelling for weakly interacting compound-forming molten alloys, to investigate the structure and chemistry of liquid Al–Cu alloys over a broad Cu concentration range. The compound-forming model (CFM) based on experimental thermodynamic data revealed the importance of the Al_2Cu "associate" in the determination of transport properties such as diffusion and viscosity as well as confirmation of the compound formation ability with regard to the available experimental data. Adequately to this fact, molecular dynamics simulation results showed strong evidence of deviation from regular metallic solution resulting from a preponderance of chemical short-range ordering, expressed by Warren–Cowley parameter and increasing abundance of icosahedral motifs with increasing Cu content. In addition, their strong impact on mass transport properties as well as the excess entropy has been detected which exhibits nonlinear compositional behaviour. Thus, we find that the Stokes–Einstein relation is unsuitable for atom transport properties determination at investigated Cu concentration range, while the Green–Kubo formalism can fully account for the experimentally observed physical phenomena. We obtain a compact and compatible view onto the structure and chemical behaviour, including atom kinetics and thermodynamics, of Al–Cu liquid alloys, which allowed us to find another hard-sphere-like metallic system in which transport properties and thermodynamics are strongly affected by packing effects. The hybrid approach presented herein gave a broader and deeper look into the liquid state of the Al–Cu alloys being missing in the literature.

Address correspondence to E-mail: trybulamarcela@wp.eu; m.trybula@imim.pl

🖄 Springer

Introduction

Precise determination of structural and chemical properties of metallic systems is strenuous, and sometimes, even impossible, due to the technical limitations of the experimental set-up. However, a database limited to one property or even an incomplete experimental dataset can usually be sufficient to perform molecular dynamics simulations and/or use CALPHAD-type models enabling to quickly cover broad compositional dependence. Recent literature reports gave proof of MD simulations being sufficient, and then, such simulations have been extensively used for studies of structure, dynamics and thermodynamics of liquid and solid bulk materials [1–6]. Sometimes MD simulations are insufficient to obtain information that can be straightforwardly retrieved from CALPHAD calculations. This is a result of CALPHAD-type models' ability to give a first insight into the structure and atomic transport properties of a melt without any knowledge of semiempirical potentials [7–10].

At least four intermetallic phases (θ-Al$_2$Cu, η-AlCu, γ-Al$_4$Cu$_9$, β-b.c.c.) exist in solid state of the Al–Cu system [11], which makes it interesting according to experimental and computational contributions given in the literature [12–14]. In contrast, only a few reports are related to the liquid phase. Rybicki et al. [15] were the first to experimentally study the structure of the liquid Al$_{83}$Cu$_{17}$ alloy, observing how the atomic groups are linked to each other. Later, this melt was the subject of computational investigations, including ab initio molecular dynamics (AIMD) [16] and classical molecular dynamics studies [5], employing MEAM potentials [17]. Consequently, both studies revealed short-range order presence in the liquid state of the Al$_{80}$Cu$_{20}$ alloy, which is responsible for anomalous structural dynamics. Similarly to the Al$_{80}$Cu$_{20}$ melt investigations, analogous computational techniques have been used for liquid structure study at an another Al–Cu alloy composition, i.e. Al$_{60}$Cu$_{40}$, including AIMD and CMD simulations performed by Wang et al. [18] and Dziedzic et al. [19], respectively.

Thermophysical properties of liquid Al–Cu alloys also caught scientific interest [19–22], including experimental and modelling contributions, which altogether build a solid background and open up a field for discussion of the new data presented in this paper. Schick et al. [20] experimentally determined viscosity for a series of liquid Al–Cu alloy compositions, excluding only the liquid Al$_{60}$Cu$_{40}$ alloy, using a high-temperature oscillating-cup viscometer method and supplementing it with thermodynamics-based modelling analyses. As a result, a pronounced maximum in viscosity was observed for Al–Cu alloy composition close to intermetallic phases existing in the solid state of the Al–Cu system, which could suggest "associates" influence. This issue has not been discussed in the literature with regard to structure and diffusivity investigations. The latter ones include the determination of the self-diffusion coefficient of Cu and of the mutual diffusion coefficient using neutron scattering [21] or X-ray radiography [22] for liquid Al-rich alloys, namely Al$_{90}$Cu$_{10}$, Al$_{83}$Cu$_{17}$, Al$_{80}$Cu$_{20}$ and Al$_{75}$Cu$_{25}$.

The "associate forming tendency" has been partially studied by Trybula et al. [23], using the free volume model (FVM), but this investigation provided only fragmentary insights into the structure and thermodynamics of Al–Cu liquid alloys. Unfortunately, those results were not enough to fully describe the physical phenomena occurring in the liquid state of the Al–Cu alloys due to the FVM constraints [24]. Apart from that, no detailed study on the topology of local atom environment and its relationship with chemistry and atom kinetics has been given yet, which could play a vital role in the investigation of glass or crystal state stability. As it has been shown in a recent study on liquid Al–Zn alloys [4], a combination of MD simulations with thermodynamics-based modelling can successfully account for experimental data and describe the relationship between the structure and thermophysical properties. One of the widely used thermodynamics-based models is the quasi-chemical approximation [7], which can successfully reproduce experimental data for various liquid metallic alloys [25, 26].

In this work, we propose to combine molecular dynamics simulations with thermodynamics-based models to study the structure and chemistry of liquid Al–Cu alloys. Furthermore, the results presented herein extend the applicability of the new modified embedded atom model (MEAM) parametrization established by Trybula [5] to Al–Cu alloys with higher Cu content. In this concept, we would like to initially compute properties that are available in the literature to check the validity of the MEAM potential. We then proceed to investigate the energetic

stability of atomic clusters and their influence on kinetics and thermodynamics of Al–Cu alloy liquid state. Structural characterization obtained by performing MD simulations concerns the analysis of local chemical surroundings of atoms, including the computation of a structure factor and pair distribution functions, which is then supplemented by 3D imaging of local atom topology. In addition, we search for a structure–dynamics–thermodynamics relationship by considering the universal scaling law [27] and extended Enskog collision frequency theory [28]. Finally, the main scope of the present work is building a bridge between MD-based simulations and CALPHAD-type modelling based on quasi-chemical approximation for a weakly compound-forming molten alloy [29] and tests it on liquid Al–Cu alloys that will be helpful in discussion of structure and chemistry of the Al–Cu system liquid state.

Computational methods

Quasi-chemical approximation for weak compound-forming melt

Within the compound formation model (CFM), the presence of an appropriate chemical compound of A_mB_n type (m and n are integer numbers) is considered for a binary system, A–B. A_mB_n type corresponds to one of the intermetallic phases occurring in the solid state, or it is just a hypothetical one. The complete mathematical formalism of the CFM approach can be found elsewhere [7, 30].

The principal thermodynamic quantity is Gibbs free energy of mixing, G_{mix}, which has the form:

$$G_{mix} = k_B T \left[\left(\frac{W}{k_B T} \right) \cdot C(1-C) + \left(\frac{\Delta W_{AB}}{k_B T} \right) \cdot \Phi_{AB}(C) \right.$$
$$\left. + \left(\frac{\Delta W_{AA}}{k_B T} \right) \cdot \Phi_{AA}(C) + \left(\frac{\Delta W_{BB}}{k_B T} \right) \cdot \Phi_{BB}(C) \right].$$

(1)

Such form of G_{mix} is obtained when standard thermodynamic relations are applied, and some algebraic rearrangements are made according to a receipt previously used by Novakovic et al. [10, 26] or Trybula et al. [9]. Φ_{ij} ($i,j = A,B$) are concentration functions depending on m and n values, C is concentration of one component, k_B is the Boltzmann constant, and T is absolute temperature. $W, \Delta W_{AB}, \Delta W_{AA}, \Delta W_{BB}$ are energy-pair parameters optimized by utilizing the

least-squares method and fitting the modelled G_{mix} to experimental one. Different expressions can be devised for the computation of the concentration functions in relevance to the assumed type of clusters existing in the liquid state. In present consideration, we examined two variants of Φ_{ij} functions, the first corresponds to the Al_2Cu compound, while the latter variant is the Al_2Cu_3 phase. Therefore, Φ_{ij} functions are formulated as follows [31]:

1. $m = 1$ and $n = 2$ for Al_2Cu compound:

$$\Phi_{AB} = \frac{1}{6}(1-C) + (1-C)^2 - \frac{5}{3}(1-C)^3 + \frac{1}{2}(1-C)^4;$$
$$\Phi_{AA} = 0;$$
$$\Phi_{BB} = -\frac{1}{4}(1-C) + \frac{1}{2}(1-C)^2 - \frac{1}{4}(1-C)^4$$

(2a)

2. $m = 2$ and $n = 3$ for Al_2Cu_3 clusters:

$$\Phi_{AB} = \frac{13}{420}(1-C) + \frac{2}{3}(1-C)^3 - \frac{3}{2}(1-C)^4$$
$$+ \frac{2}{3}(1-C)^6 - \frac{5}{7}(1-C)^7 + \frac{1}{4}(1-C)^8;$$
$$\Phi_{AA} = -\frac{53}{840}(1-C) + \frac{2}{3}(1-C)^3 - \frac{5}{4}(1-C)^4$$
$$- (1-C)^6 + \frac{4}{7}(1-C)^7 - \frac{1}{8}(1-C)^8;$$
$$\Phi_{BB} = \frac{23}{280}(1-C) - \frac{1}{2}(1-C)^4 + \frac{2}{5}(1-C)^6$$
$$+ \frac{1}{7}(1-C)^7 - \frac{1}{8}(1-C)^8.$$

(2b)

The aforementioned functions can also be used for examining the chemical short-range order in a melt. The first structure index, that is directly calculated from the CFM formalism and linked to Bhatia–Thornton (B–Th) theory [32], is the concentration fluctuation function at the long wavelength limit, $S_{CC}(0)$. It is an indicative of chemical short-range order, and for a sub-regular metallic system it is formulated as follows:

$$S_{cc}(0) = k_B T \left[\left(\frac{W}{k_B T} \right) \cdot C(1-C) + \left(\frac{\Delta W_{AB}}{k_B T} \right) \cdot \Phi_{AB} \right.$$
$$\left. + \left(\frac{\Delta W_{AA}}{k_B T} \right) \cdot \Phi_{AA} + \left(\frac{\Delta W_{BB}}{k_B T} \right) \cdot \Phi_{BB} \right],$$

(3)

while for ideal solution, $S_{cc}(0, id)$ has the form of:

$$S_{CC}(0, id) = C(1 - C). \tag{4}$$

The second indicator of short-range order (SRO) in a molten alloy is the Warren–Cowley parameter α_{tot} [33], quantifying chemical SRO within the first coordination shell and it is written:

$$\alpha_{tot} = \frac{M - 1}{[1 - M \cdot (Z - 1)]}, \tag{5}$$

where Z is the coordination number and M is the $S_{cc}(0)/(S_{cc}(0, id))$ ratio. A melt has a compound formation tendency for which the M value is lower than unity [34].

Molecular dynamics simulations

A recent parametrization of the modified embedded atom model (MEAM), given by Trybula [5] for liquid $Al_{80}Cu_{20}$ alloys, has been used for the investigation of $Al_{1-x}Cu_x$ ($x = 10, 30, 40$ and 50 at%) alloys properties by means of molecular dynamics simulations (MD). A consistent and compact description of liquid Al_{80}-Cu_{20} alloys' properties was obtained in reference to the previous ab initio molecular dynamics [16] (AIMD) and experimental [20, 22, 35] results. Herein, we validate this MEAM parametrization for structure and transport properties investigations over a broad Cu concentration range. All MD simulations have been performed using the LAMMPS code [36] and carried out using the Verlet algorithm with a time step of 1.5 fs. Cubic box with a total number of 1372 atoms was built, and periodic boundary conditions in three directions were imposed for each Al–Cu composition investigated. Randomly oriented atoms in the simulation box were initially heated up to 2500 K and thermalized during 100 ps. Pressure, volume and temperature of each sample during quenching were monitored to reproduce experimental densities [37] at each temperature investigated ($T = 1073, 1173, 1223, 1345$ and 1523 K). Before structural and dynamic properties determination, each sample was thermalized during 20 ps and the final simulations were continued for 500 ps to determine structural and transport properties of liquid $Al_{1-x}Cu_x$ alloys investigated ($x = 10, 30, 40$ and 50 at% Cu). For structure analysis, 50 atomic configurations regularly spaced in time were selected and extracted from the MD trajectories and then were used for three-dimensional topological analysis including the Voronoi

tessellation method [38]. Each atomic structure was brought to minimum energy using the steepest descent algorithm as implemented in LAMMPS.

Self-diffusion coefficient, describing the random walk motion of tagged atomic species β ($\beta = A, B$ for A and B being the particles of an AB binary system), was determined from the linear slope of the mean square displacement (MSD), equivalent to the Green–Kubo formalism, given as:

$$D_\beta = \lim_{t \to \infty} \frac{1}{N_\beta} \sum_{i=1}^{N_\beta} \frac{\left\langle \left| \mathbf{r}_{i,\beta}(t) - \mathbf{r}_{i,\beta}(t=0) \right|^2 \right\rangle}{6t}, \tag{6}$$

where $r_{i,\beta}(t)$ is the position of particle i of species β at time t.

While for A–B binary systems various methods for computing the mutual diffusion coefficient exist, the first one is the simple Darken's relationship [39] linking the interdiffusion coefficient to self-diffusion coefficients, which is written as:

$$D_{AB} = C_B D_A + C_A D_B. \tag{7}$$

In practice, Eq. (7) is not valid for concentrated melts with a strong associate forming tendency; hence, a modified Darken's formula is used instead. It incorporates an additional thermodynamic factor, Θ [39].

The second expression that can be used for mutual diffusion coefficient computation is the universal scaling law of Dzugutov [27] that is constituted by two important assumptions. The first includes the Enskog collision frequency describing binary collisions of dense hard-sphere fluids, only restricted to short-range repulsive forces, and governing the energy and momentum transfer [28]. In our investigations, we have considered the extended Enskog's theory on a binary liquid, where reduced self-diffusion coefficient written as $D^*_i = D_i/\chi_i$ is computed using relevant diffusion scale factor of ith species in a binary liquid [40]:

$$\chi_1 = 4\sigma_1^4 g_{11}(\sigma_{11})\rho_1 \sqrt{\frac{\pi k_B T}{m_1}} + 4\sigma_{12}^4 g_{12}(\sigma_{12})\rho_2 \sqrt{\frac{\pi k_B T}{m_1 m_2}}. \tag{8}$$

Here, $g_{11}(\sigma_{11})$, ρ_1 and m_1 are partial pair-correlation functions of the hard sphere, atomic density and mass, respectively. An analogous factor is defined for second species by interchanging index 1 with 2 in Eq. (8). The second assumption relates to the

frequency of the local structural relaxations associated with diffusive atomic motions dominated by cage effect which is proportional to the number of accessible configurations. In turn, the normalized diffusion D^* is proportional to $\exp(S)$, where S is the excess entropy expressed in Nk_B units and D^* can be estimated by reformulating Eq. (8) as:

$$D^* = \left(\frac{D_i}{\chi_i}\right)^{X_1} \cdot \left(\frac{D_j}{\chi_j}\right)^{X_j}. \tag{9}$$

If the $S_{cc}(0)$ function is known, the interdiffusion coefficient of a binary liquid, D_{AB}, can also be calculated using Eq. (10a):

$$D_{AB} = \frac{S_{CC}(0)}{S_{CC}(0,\mathrm{id})} \cdot D_{\mathrm{id}}, \tag{10a}$$

$$S_{CC}(0) = k \cdot T \cdot \left(\frac{\partial^2 G_{\mathrm{mix}}}{\partial x^2}\right)^{-1}. \tag{10b}$$
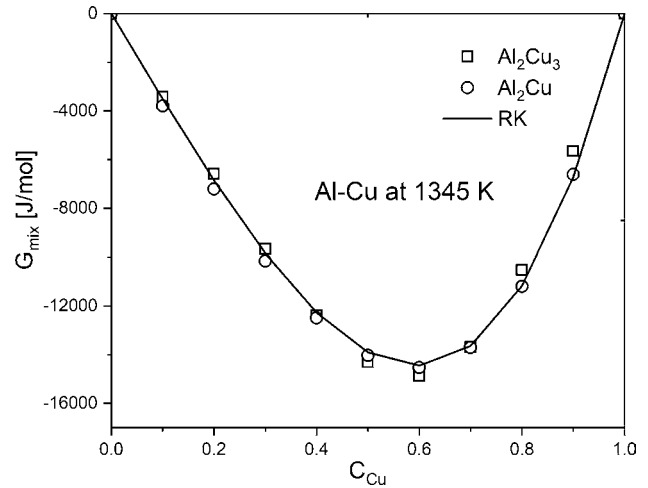
D_{id} is the chemical diffusion coefficient for an ideal mixture. Importantly, Eq (10a) explores the structure–dynamics relation involving only macroscopic thermodynamic information and links the short-range order to diffusion phenomenon [29]. G_{mix} is sum of G^{id} and G^{xc}, the latter is expressed in terms of thermodynamic parameters (L_i^{Liq}, $i = 1, 2, 3$) standing for Redlich–Kister polynomial coefficients [41].

The second important transport property, that is readily computed using molecular dynamics simulations, is shear viscosity η. It can be accessed through the Stokes–Einstein relation [42] [Eq. (11a)] or Green–Kubo formalism [43] [Eq. (11b)], both of them describe the collective motion of a macroscopic particle and are formulated as:

$$\eta_{\mathrm{SE}} = \frac{k_B T}{6 \cdot \pi \cdot D_{AB} \cdot R} \tag{11a}$$

$$\eta_{\mathrm{GK}} = \frac{1}{k_B \cdot T \cdot V} \int_0^\infty \langle \sigma^{xz}(t) \cdot \sigma^{xz}(0) \rangle \, \mathrm{d}t. \tag{11b}$$

Here σ^{xz} is an off-diagonal element of the stress tensor computed by averaging over time, and similar averages are computed for the equivalent yz and xy components of the stress tensor. R corresponds to the position of the first maximum of the radial distribution function.

Figure 1 Computed integral Gibbs energy of mixing as a function of Cu concentration at 1345 K using CFM formalism with assumption of: circle Al_2Cu and rectangle Al_2Cu_3 "associate" type, solid line—RK polynomial [44].

Results and discussion

Thermodynamics-based modelling

Keeping in mind the brief description of the CFM method, the mixing Gibbs free energies (G_{mix}) were computed at 1345 K assuming the presence of two "associate" types, i.e. Al_2Cu and Al_2Cu_3; the results are plotted in Fig. 1. The interaction energy parameters W_{ij}, used for fitting Gibbs free energy to the one computed employing the Redlich–Kister (RK) polynomial (solid line in Fig. 1), are given in Table 1 in the form of their temperature dependence for both associate types considered. Here, the RK's Gibbs energies are those computed using thermodynamic parameters ($^iL^{\mathrm{Liq}}$, $i = 0, 1, 2, 3$) taken from Witusiewicz et al. [44] to Redlich–Kister polynomial [41] and they are collected in Table 1.

Two important features can be read from Fig. 1, with regard to the G_{mix} minimum position and the convergence of the experimental points with those obtained from CFM computations. First of all, for both atomic cluster assumptions used for CFM, the G_{mix} minimum position was located at the same Cu concentration (the $Al_{40}Cu_{60}$ alloy). Secondly, consideration of the Al_2Cu atom cluster gives a slightly better agreement of CFM-based G_{mix} with the RK's G_{mix} as opposed to the second atomic cluster considered in this work.

Table 1 Cluster types, interaction parameters W, W_{AB}, W_{AA} and W_{BB} used for CFM model and thermodynamic parameters of the Gibbs energy of Al-Cu liquid phase [44]
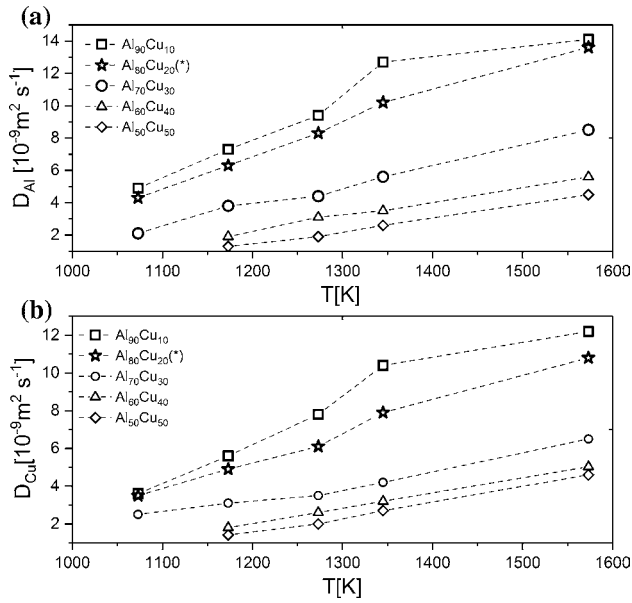
Cluster	W (J mol^{-1})	W_{AB} (J mol^{-1})	W_{AA} (J mol^{-1})	W_{BB} (J mol^{-1})
Al$_2$Cu	$-39.2 - 0.0558 \times T$ $+ 3E{-}5 \times T^2$ $- 6E{-}9 \times T^3$	$-5.92 + 0.011 \times T$ $- 6E{-}6 \times T^2$ $+ 1E{-}9 \times T^3$	0	$-0.398 - 0.013 \times T$ $+ 6E{-}6 \times T^2$ $- 2E{-}10 \times T^3$
Al$_2$Cu$_3$	$215.1 - 0.0506 \times T$ $+ 4E{-}6 \times T^2$ $- 1E{-}10 \times T^3$	$-570.2 + 0.120 \times T$ $- 8E{-}6 \times T^2$ $+ 2E{-}10 \times T^3$	$-668.2 + 0.147 \times T$ $- 1E{-}5 \times T^2$ $+ 3E{-}10 \times T^3$	$-3E6 + 692.88 \times T$ $- 0.053 \times T^2$ $+ 1E{-}6 \times T^3$

Thermodynamic parameters of Al–Cu liquid phase (J K^{-1})
$^0L^{Liq} = -67{,}094 + 8.555T$
$^1L^{Liq} = 32{,}148 - 7.118T$
$^2L^{Liq} = 5915 - 5.889T$
$^3L^{Liq} = -8175 + 6.049T$

Diffusivity: CFM computation versus MD simulations

Below, we report the self-diffusion (SD) coefficients of each species composing Al–Cu alloys and the mutual diffusion coefficient. The temperature dependence of the SD coefficient for Al and Cu species is graphically presented in Fig. 2a, b, respectively. One can observe that the SD coefficients of both Al and Cu species exhibit significant deviation from a linear dependence for Cu-deficient content of Al–Cu alloys which becomes linear again for Cu-enriched alloys. An isotherm of *SD* coefficients computed at 1345 K for Al and Cu atoms in liquid Al–Cu alloys is plotted in Fig. 3, which includes also *SD* coefficients taken from Meyer et al. measurements for Al [45] and Cu [46] and represented by diamonds. Therefore, a significant difference in the SD coefficient values between Al and Cu atomic species can be easily seen from Fig. 3 for the investigated Al–Cu liquid alloys. Another striking feature is an appreciable decrease in SD coefficients between 10, 20 and 30 at% Cu content as demonstrated in Fig. 2a, b. Such changes could be attributed to the variety of intermetallic phases present in solid Cu-rich Al–Cu alloys, in which the Al atoms are more likely to be chemically bonded to Cu atoms compared to the Al-rich alloys. Regarding the concentration-dependent SD coefficient of Al, the present MEAM-MD simulations predict its almost linear decrease with increasing Cu content in liquid Al–Cu alloys. A substantial disagreement is found between the present studies and the AIMD data of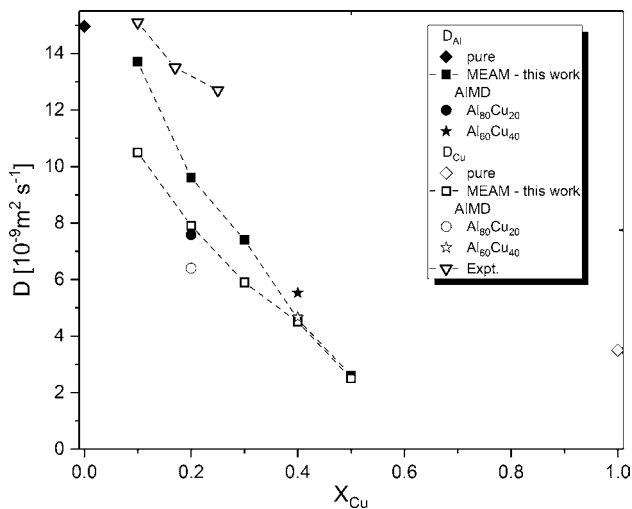 Wang et al. [16], which particularly concerns the Al$_{80}$Cu$_{20}$ alloy, and this issue has been previously discussed by Trybula [5]. Interestingly, SD coefficient of Al in liquid Al–Cu alloys has attracted less scientific attention compared to that of copper, and this produces some difficulty in its discussion. In the case of SD coefficient of Cu species, investigated for selected binary Al–Cu alloys and drawn in Fig. 3, the MEAM-MD simulations also give its linear change and demonstrate a very good agreement with previous AIMD simulations performed for the liquid Al$_{60}$Cu$_{40}$ [18] and Al$_{80}$Cu$_{20}$ alloys [16]. Such observation does not apply to experimental data by Dahlborg et al. [21], whose values are substantially higher than both MEAM-MD and AIMD simulations results. To our best knowledge, no regular studies on diffusivity over a broad Cu concentration range using a single computational or experimental technique have been performed so far, which introduces a slight difficulty in their validation.

The mutual diffusion coefficient of Al–Cu liquid alloys is drawn as a function of Cu concentration in Fig. 4. The linear change in observed composition dependence of self-diffusion coefficients is incompatible with that observed for the mutual one which is observed for the present MEAM-MD simulation results and CFM calculations, as it is illustrated in Fig. 4. Indeed, MEAM-MD and CFM-Al$_2$Cu calculations give results quite close to each other compared to an appreciable difference recorded for the CFM-Al$_2$Cu$_3$ data. The most striking feature in D_{AB} coefficient behaviour is seen for Al-rich alloys: it consists in a nonlinear decrease of the D_{AB} coefficient with increasing Cu content which gradually changes over

Figure 2 a, b Temperature-dependent self-diffusion coefficients of Al and Cu atomic species of liquid Al–Cu alloys, respectively.
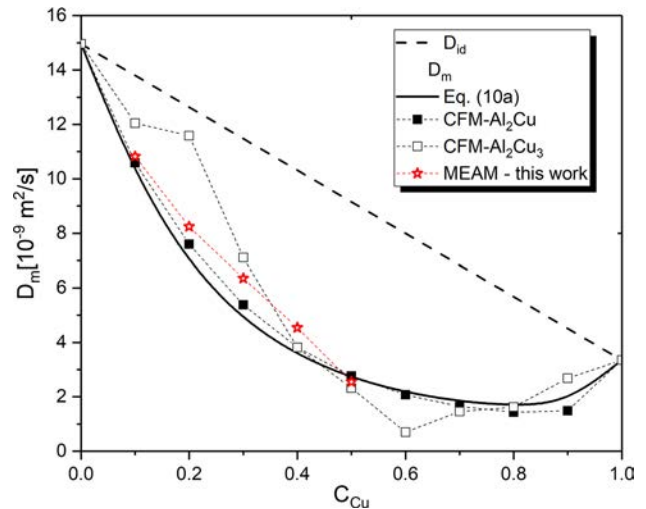
to a slight increase near the $Al_{40}Cu_{60}$ alloy composition. When CFM calculation results for D_{AB} coefficient are confronted with the ones computed using Eq. (10a), the CFM-Al_2Cu results appear to correlate well with Eq. (10a) compared to MEAM-MD simulation data exhibiting a worse agreement. Apart from that, both "associate" assumptions employed in the CFM formalism, MEAM-MD simulation and Eq. (10a), are consistent in describing the negative
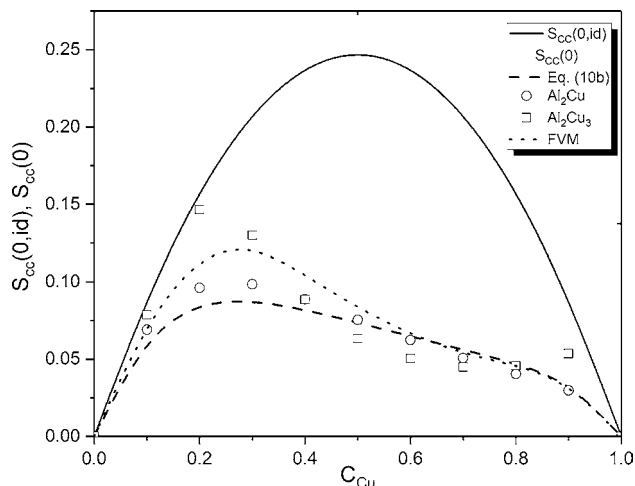
deviation from linearity represented by a long-dashed line in Fig. 4, corresponding to the chemical diffusion coefficient of ideal solution, D_{id}. The extended Darken's formulation has also been considered in our investigation for estimation of the D_{AB} coefficient. However, it gave significantly overestimated D_{AB} coefficients for Al–Cu liquid alloy compositions in the vicinity of the intermetallic phases existing in solid state and consequently, they have not been depicted in Fig. 4. According to Trybula et al. studies [9], the assumption of A_2M_3 "associate" type enables one to predict a nonlinear change in mutual diffusion coefficient, even if various arbitrary parameters are used. Importantly, its curvature is synchronized with the shape of $S_{cc}(0)$ function correlating with the thermodynamic driving force. As will be shown below, the two assumptions used in this work give two different descriptions of the fluctuation function for the liquid $Al_{80}Cu_{20}$ alloy. To prove the aforementioned statement, we need to have complete information derived from structural studies that will also be presented below.

Since a direct method for the determination of the concentration fluctuation function using molecular dynamics simulations has not been given yet, and its experimental determination is extremely difficult, first we try to discuss the data obtained using CFM formalism in our previous study [9], plotted in Fig. 5. Two different formalisms have been used for the thermodynamics-based computations, that is FVM

Figure 3 SD coefficients isotherm as a function of Cu concentration computed at 1345 K. AIMD data—$Al_{80}Cu_{20}$ [16] and $Al_{60}Cu_{40}$ [18], diamonds—expt. data for pure elements [45, 46], and asterisk—simulation data taken from [5].

Figure 4 Mutual diffusion coefficient computed: squares—CFM formalism [Eq (7)], long-dashed line—D_{id}; solid line—Eq. (10a), and red stars—MEAM-MD simulations. Lines are guide to the eye.

Figure 5 Concentration fluctuation function in the long-wave limit, $S_{cc}(0)$: solid line—ideal solution, dashed line—B–Th model [Eq. (10b)] [47], whereas symbols—modelled data at 1345 K: open triangles—CFM formalism, and stars—MEAM-MD data.

[4] and CFM (this work), which gave quite similar $S_{cc}(0)$ function behaviour. In our present CFM computations, other atomic clusters have also been considered; however, we dismissed them from further discussion due to significant misfits in mixing thermodynamic properties giving an unrealistic description of concentration fluctuation and dynamic properties. Since the Al_2Cu "associate" type is considered, a flat maximum located around 30 at% of Cu is observed along with almost perfect agreement to the approximated experimental $S_{CC}(0)$ function (dashed line in Fig. 5). The latter has been assessed by using Eq. (10b) with $G_{mix} = (G^{xc} + G^{id})$ calculated using the RK polynomial. At the same time, consideration of the Al_2Cu_3 cluster allows us to observe a sharp maximum at 20 at% Cu content and a minimum spanned over 60–80 at% Cu. Importantly, the CFM formalism with assumption of the Al_2Cu_3 "associate" predicts the $Al_{90}Cu_{10}$ and $Al_{80}Cu_{20}$ alloy to be ideal solutions, while both FVM and CFM-Al_2Cu computations as well as B–Th theory data contradict such behaviour. The latter have been computed as a second derivative of mixing Gibbs free energy with respect to concentration—Eq. (10b) [47]. Despite this fact, a substantial disagreement between FVM and CFM-Al_2Cu calculations is seen for Al-rich Al–Cu alloys when they are confronted with B–Th results (dashed line in Fig. 5).
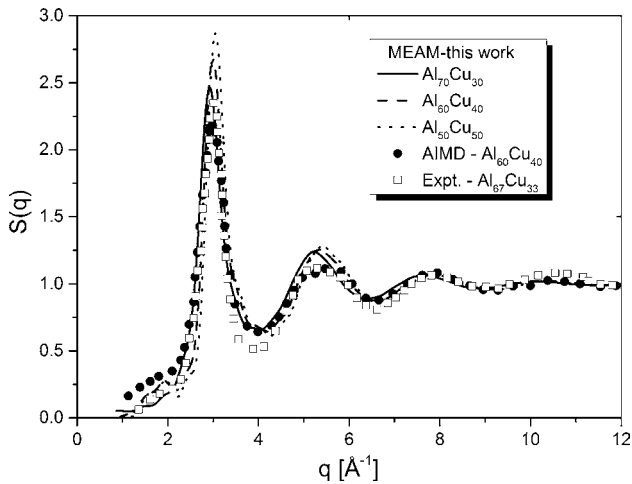
The CFM-Al_2Cu calculation gives a significantly smaller discrepancy from the approximated

experimental data in comparison with the CFM-Al_2Cu_3 results. Such a good correlation undoubtedly gives the first evidence of Al_2Cu associate importance, and it might suggest their preponderance in liquid Al–Cu alloys. Indeed, the trend observed in $S_{cc}(0)$ change is compatible with the one that can be read from the phase diagram [11], namely intermetallic phase absence on the Al-rich side of the phase diagram corresponds to the appearance of $S_{cc}(0)$ maximum in comparison with a smooth decrease observed for high-Cu-content Al–Cu liquid alloys. The present MEAM-MD simulations give slightly higher values of the $S_{cc}(0)$ function compared to the CFM-Al_2Cu calculations and experimentally predicted data. However, they are still lower than line representing the ideal solution and, importantly, this does not change the structural description of liquid Al–Cu alloys. Because the $S_{cc}(0)$ function values for Al–Cu liquid alloys are lower than for ideal solution $(S_{cc}(0)/S_{cc}(0, id) < 1)$, the Al–Cu alloys rather have a tendency for compound formation according to the definition given by Bhatia and Thornton [47]. In turn, the present CFM-Al_2Cu and MEAM-MD simulation results are in line with this observation and FVM computation data [23] over the whole range of Cu concentrations investigated, as opposed to the selected ones found by our present CFM-Al_2Cu_3 calculation.

Structure and local atomic arrangements: molecular dynamics study

The structure factors $S(q)$ for a series of liquid Al–Cu alloy compositions investigated in this work are plotted in Fig. 6 and confronted with X-ray experimental data measured by Brillo et al. [48] (black squares) and AIMD simulation results [16] (open circles). The $S(q)$ values for each of the studied Al–Cu alloys exhibit a pronounced, narrow first peak becoming much more intense with increasing Cu content, while negligible differences in damped oscillations are seen for the second and third peaks. Such changes signify that Al–Cu alloys become more densely packed liquids with increasing Cu content and inform about the loss of randomness in atomic packing of Al–Cu alloys, that is also compatible with the observed decrease in $S_{cc}(0)$ function and the analysis of the Al–Cu phase diagram. Indeed, the existence of at least four different copper-rich intermetallic phases (θ-Al_2Cu, η-AlCu, γ-Al_4Cu_9, β-Bcc)
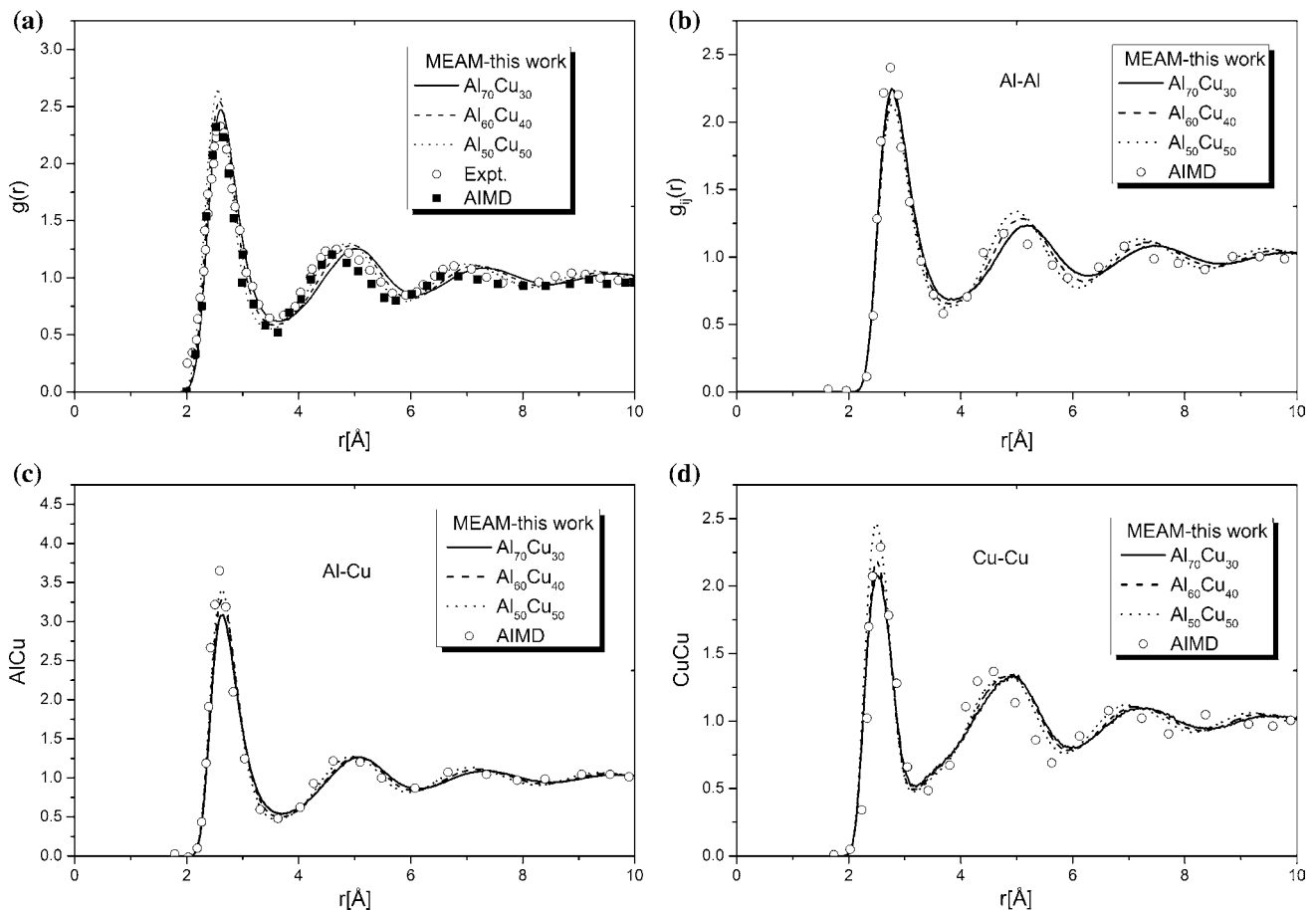
Figure 6 Structure factor of liquid $Al_{1-x}Cu_x$ alloys: solid, dashed and dotted lines represent MEAM data for x equal to 30, 40 and 50 at%, respectively. Open circles and black squares—AIMD results for liquid $Al_{60}Cu_{40}$ [18] and X-ray experimental data for liquid $Al_{67}Cu_{33}$ alloy [35], respectively.

[44] can imply on observing an increase in alloy ordering. The MEAM-MD simulations data are in acceptable agreement with available experimental results for the $Al_{67}Cu_{33}$ liquid alloy measured at 1023 K [35] and AIMD simulations performed for the $Al_{60}Cu_{40}$ liquid alloy at 1323 K [18], as position of the first peak is considered. A slightly different scenario can be perceived from the trend in intensity change of the first peak of $S(q)$ (Fig. 6). The MEAM-MD simulations show its increase with increasing Cu content, while AIMD simulations gave a less intense first peak compared to the experimental data.

Interestingly, MEAM-MD computations allow us to observe a weak pre-peak occurrence at short q for liquid $Al_{1-x}Cu_x$ alloys for $x = 0.3$, 0.4 and 0.5 which can also be seen for X-ray and AIMD data in comparison with its absence in the $Al_{80}Cu_{20}$ liquid alloy [16]. Analogous observations emerge from the analysis of total pair-correlation function of liquid Al_{1-x}

Figure 7 a Total and **b-d** partial pair distribution functions for selected liquid Al–Cu alloys. Solid, dashed and dotted lines—MD simulations for liquid $Al_{70}Cu_{30}$, $Al_{60}Cu_{40}$ and $Al_{50}Cu_{50}$, respectively; symbols (open circles)—AIMD data [16] and (full squares)—experiment [35].

Table 2 Symbol, method and coordination number

Z	Method	Coordination number			
		$Al_{90}Cu_{10}$	$Al_{70}Cu_{30}$	$Al_{60}Cu_{40}$	$Al_{50}Cu_{50}$
Z_{Al}	MEAM	11.74	12.68	13.32	13.47
Z_{Cu}		10.99	10.95	11.17	10.97
Z_{tot}		11.06	11.47	12.03	12.22

Table 3 Methods used and chemical short-range order parameter (CSRO)

Method	CSRO			
	$Al_{90}Cu_{10}$	$Al_{70}Cu_{30}$	$Al_{60}Cu_{40}$	$Al_{50}Cu_{50}$
MEAM-MD	− 0.041	− 0.126	− 0.158	− 0.172
CFM-Al_2Cu	− 0.031	− 0.102	− 0.145	− 0.188
CFM-Al_2Cu_3	− 0.015	− 0.148	− 0.193	− 0.231
B–Th	− 0.035	− 0.111	− 0.154	− 0.194

Cu_x alloys for $x = 0.3$, 0.4 and 0.5 drawn in Fig. 7a. Some insignificant mismatch between present MEAM-MD results and available literature data is found, concerning the intensity of the first peak and shape of the second and higher-order peaks, whereas the position of the first peak is moving towards shorter interatomic distance with Cu content growth and approaching to that measured by Shtablavyi et al. [15] for pure Cu element. For clarity of Fig. 7a, MEAM and AIMD data for the liquid $Al_{80}Cu_{20}$ alloy are not appended; they are discussed in detail elsewhere [5].

Partial pair-correlation functions, contributing to the total correlation function, $g(r)$, that is $g_{AlAl}(r)$, $g_{AlCu}(r)$, $g_{CuCu}(r)$, are graphically presented in Fig. 7b-d, correspondingly. As it can be seen, MEAM-MD data also show high consistency with X-ray diffraction [35] and AIMD simulations data [16, 49] with exception of the g_{CuCu} partial. According to our recent observation made for the $Al_{80}Cu_{20}$ liquid alloy [5], an adequate inconsistency in the position and shape of the high-order peaks in $g_{CuCu}(r)$ partial has also been found. Therefore, it might mean that the atomic pair interactions described within MEAM method potential for Cu element need to be treated more attentively, which is beyond the scope of the present work. Apart from the slight inconsistency exhibited by the MEAM-MD data, any splitting of the second peak has not been seen for each of the $g(r)$ partials. If it had been observed, such peculiarity would have been suggestive of the icosahedral short-range ordering [16]. Interestingly, both experimental and AIMD data support the $S_{CC}(0)$ function discussed above, which provides information that will be essential in further discussion concerning the topological local atom surrounding study.

By integration of each partial $g_{ij}(r)$ up to the first minimum, average partial and total coordination numbers (CN) were computed; they are collected in

Table 2. The average total CN for the investigated liquid Al–Cu alloys increases with increasing Cu content, and importantly, and such trend is compatible to that displayed by AIMD simulations for $Al_{80}Cu_{20}$ and $Al_{60}Cu_{40}$ liquid alloys [16, 18]; however, it is less pronounced. A significant rise in total coordination number obtained by performing MEAM-MD simulations can signify the occurrence of structural changes in atomic packing of liquid Al–Cu alloys with Cu content growth. As it can also be seen, MEAM potential overestimates both experimental and AIMD data resulting from highly coordinated Al central atoms. It needs to be stressed that the MEAM potential usually gives higher coordination numbers with regard to experiment or AIMD data due to its sensitivity to the first minimum position of $g_{ij}(r)$ [5]. Importantly, recent experimental reports delivered a quite different look into the relationship between CN and Cu composition. The CNs increase substantially with increasing Cu content between 17 and 34% of Cu–$Al_{83}Cu_{17}$ and $Al_{66}Cu_{34}$ alloys [35]. A similar relationship to that observed for our present MEAM-MD simulations has found confirmation in a previous study of Al-Ni liquid alloys structure for which total and partial CNs increase with increasing Ni content [1]. Due to the similarity in thermodynamic and/or physicochemical properties' concentration and temperature dependences [50], similar trend in CNs change is also expected to be seen for the Al–Cu liquid alloys.

Taking into account the information presented above, the atomic short-range order can be quantified by computing the Warren–Cowley parameter (α). Therefore, we compared all thermodynamics-based estimations—Eq. (5) and B–Th model [Eq. (10b)] with MEAM-MD simulations. For the latter case, we used random-packed model [51] defining the parameter α_{tot} as:

$$\alpha_{\text{tot}} = \frac{c_{\text{Cu}}(Z_{\text{Al-Al}} - Z_{\text{Cu-Al}}) + c_{\text{Al}}(Z_{\text{Cu-Cu}} - Z_{\text{Al-Cu}})}{Z_{\text{tot}}}.$$
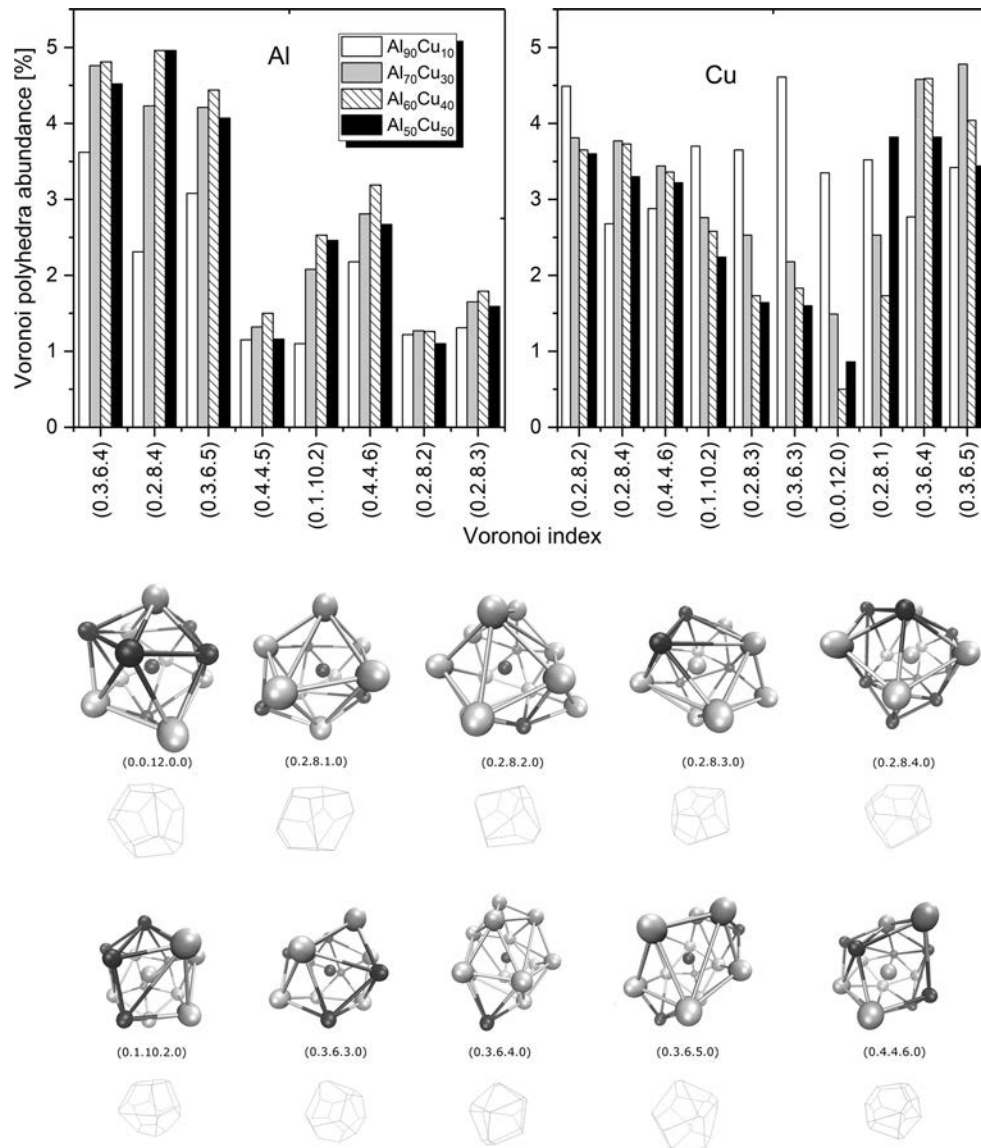
(12)

The quantified chemical short-range order (CSRO) is gathered in Table 3 for MEAM-MD simulations data, CFM computations and available literature data [30] computed at 1345 K.

CFM computations performed assuming Al_2Cu and Al_2Cu_3 give negative CSRO parameter, and therefore, its sign confirms the presence of chemical ordering in the liquid Al–Cu alloys which does increase with growing Cu content. As it can be seen, CFM-Al_2Cu calculations predict slightly higher CSRO parameter compared to the one estimated using Eq. (10b) and experimental thermodynamic data [30]. For further comparison, a recent study of Das et al. [52]. provided some interesting observations related to chemical description of liquid Al–Ni alloys, involving diffusion and CSRO. Basically, the nonlinear compositional dependence of diffusion coefficients corresponds to increasing CSRO, moving towards the Ni-rich side. Note that a similar relationship is exhibited by the analysed liquid Al–Cu alloys, namely the growth in CSRO with increasing Cu content reflects in decreasing self- and mutual diffusion coefficients. By definition, the CSRO parameter describes chemical local atom environment; therefore, its increase informs that liquid structure becomes densely packed reflecting in a significant deviation from random atom ordering. Such behaviour is a good example of the hard-sphere-like liquids behaviour, for which mass transport is strongly correlated with packing fraction of atoms [53, 54]. To have a complete view onto the mass transport property, we decide to extend our consideration on viscosity investigation, which will be discussed in the following section.

Three-dimensional analysis based on the Voronoi tessellation was performed, in which a geometrical construction divides the investigated space into polyhedra, containing a single atom, called Voronoi cells (VC). The local atom topology as a function of composition and temperature is inspected. Within Voronoi analysis, the total number of the VC faces corresponds to the coordination number assigned to the central atom. Voronoi index $n_3, n_4. n_5, n_6, \ldots$ is used to differentiate between the VC types, where n_i is the number of i-edged sides in the polyhedron. This structural tool allows to distinguish body- and

face-centred cubic (b.c.c. and f.c.c.), as well as hexagonal close-packed (h.c.p.) structures. Further details on the Voronoi tessellation method, they can be found elsewhere [55, 56]. Ten types of Voronoi cells (VC) are found to be in reasonable abundance among the 100 different types of cells around Al and Cu atomic species in liquid $Al_{1-x}Cu_x$ ($x = 10, 30, 40$ and 50) alloys at 1345 K. VCs abundance and their geometrical construction are drawn in Fig. 8.

High coordination numbers around Al and Cu species correspond to high-indexed Voronoi cells (VCs). As compared to the AIMD data at 1345 K for the $Al_{60}Cu_{40}$ liquid alloy [49], some similarities have been found concerning abundance and cluster types distinguished in the Al–Cu liquid alloys examined. At first, icosahedral clusters of $< 0\ 0\ 12\ 0 >$ index—ideal icosahedron are found to be not the most abundant index compared to distorted icosahedra of $\{< 0\ 1\ 10\ 2 >, < 0\ 3\ 6\ 4 >\}$. It is argued that local icosahedral structures have a positive influence on stabilization of undercooled liquid state [57] resulting from their compact structure; therefore, we can expect that this issue is also applied to liquid Al–Cu alloys. On the other hand, their preponderant abundance has a beneficiary influence on slowing down relaxation processes distinguished during glass transition. Compact structures, like icosahedra derivatives, can be responsible for slow structural dynamics compared to loosely packed clusters undergoing fast structural dynamics [58, 59] resulting in significantly displacing local atom regions. Recognizable discrimination in VCs as it has been found between Al and Cu local surrounding could have indicated that liquid Al–Cu alloys undergo two relaxation processes. Invoking at this moment the previously discussed functions, representing chemistry of local atom surrounding: structure factor and distribution function, any evidence of middle-range ordered clusters has not been found. Therefore, it can be stated that Al–Cu liquid alloys undergo processes which enable liquid materials to crystallize rather than have an amorphous structure, excepting only the Al-rich alloys, due to the existence of a number of interatomic phases stabilizing the solid state of the Al–Cu system [11]. Quite interestingly, such a conclusion was confirmed by Wang et al. [16]; in particular, the liquid $Al_{80}Cu_{20}$ alloy can be classified as a strong liquid according to Angel classification [60] with fragility value lower than 10 that provides a
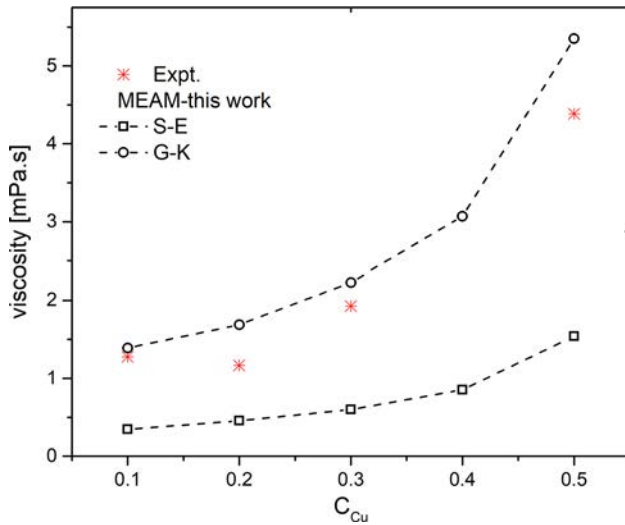
Figure 8 The abundance of Voronoi cells (top) found at 1345 K around Al and Cu species in liquid Al–Cu alloys and their geometrical construction (bottom).

straightforward suggestion of weak glass forming ability.

Viscosity

For viscosity determination, at first, we confine our investigation to test the validity of Stokes–Einstein (S–E) [42] relation for Al–Cu liquid alloys using only MEAM-MD data. Its compositional dependence is shown in Fig. 9. As compared to the experimental data collected by Brillo [48], the inability of S–E relation to accurately reproduce the experimental data (red stars) can be easily seen which corresponds to a substantial underestimation of experiment. Such behaviour eliminates the S-E equation consideration from further studies of liquid Al–Cu alloys in contrast to the simple liquids, for which this relation is obeyed. Consequently, we employ the Green–Kubo (G–K) formalism [43] [Eq. (11b)] as previously Asta et al. [61] used for liquid Al–Ni alloys investigation. Importantly, the G–K approach (circles) allows to get an overall 5–15% agreement with the experiment over a broad Cu concentration range.

Figure 9 MEAM MD computed (full and empty squares) and measured (stars) viscosity at 1345 K as a function of Cu concentration. Experimental data were taken from Brillo et al. [48]. Lines are guide to the eye.

The nonlinear behaviour of viscosity is strongly correlated with nonlinear diffusion coefficients change as a result of the CSRO degree increasing with Cu content growth. Quite interestingly, the experiment also exhibits the same behaviour [21], compared to an almost complete failure given by the S–E relation. On the Al-rich side, where no intermetallic phases exist, viscosity slightly decreases towards the $Al_{80}Cu_{20}$ alloy and suddenly increases as the Al_2Cu compound starts to form [11]. In turn, an estimation of the fragility parameter [60, 62, 63] is not necessary

due to a negligible evidence of icosahedral motifs or Wang et al. remarks [16] as well as significant Al_2Cu compound influence stimulating the solidification of liquid Al–Cu alloys [14, 64–66].
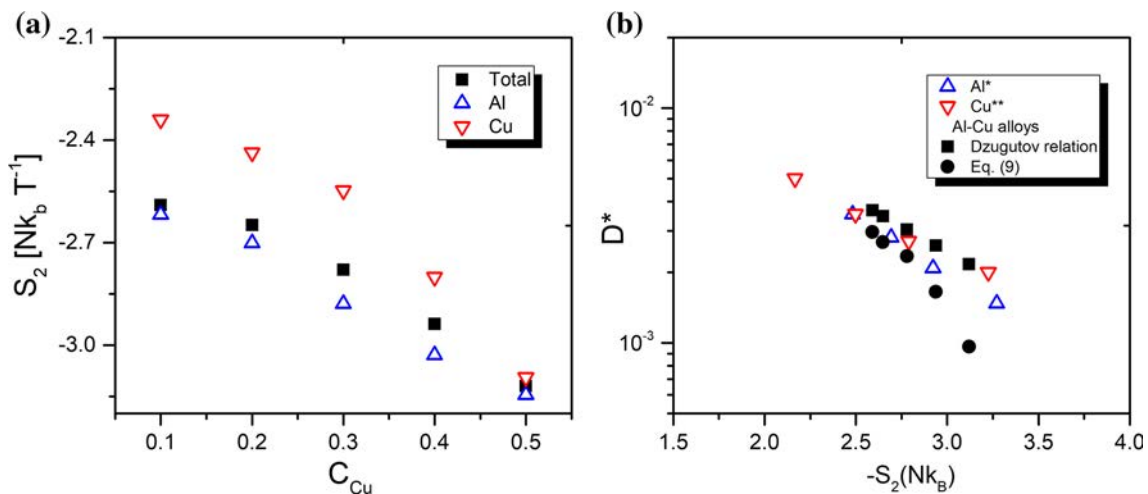
Excess entropy

To define the structure–dynamics relationship in liquid Al–Cu alloys, we considered the universal scaling law relating diffusion coefficient to compute the excess entropy as formulated in the original work by Dzugutov [27]. In the frame of this formulation, the excess entropy (expressed in k_B units) is restricted to a two-body contribution:

$$S_2 = -2\pi\rho \int_0^\infty \{g(r)\ln[g(r)] - [g(r) - 1]\} r^2 dr, \qquad (13)$$

for ρ being the number density. In other words, Dzugutov scaling law is an important contribution combining the kinetics of a liquid to a static thermodynamic quantity, S. In our case, it is S_2 function coupled to an accessible structural property of a liquid—partial pair-correlation function, whereas the total excess entropy is given by $S_2 = X_{Al} S_2^{Al} + X_{Cu} S_2^{Cu}$, where S_2^{Al} and S_2^{Cu} are partial molar entropy of Al and Cu atoms, respectively. The partial and total S_2 function computed at 1345 K are plotted in Fig. 10a.

For the investigated Al–Cu alloys, we observe a decrease in total excess entropy (S_2) with increasing Cu content as well as substantial discrimination in

Figure 10 a Computed total and partial entropies (S_2) as a function of Cu composition at 1345 K and **b** scaled diffusion versus entropy for liquid Al–Cu alloys and pure elements: Al [27] and Cu [61].

partial entropy between Al and Cu elements on the Al-rich side which decreases with increasing Cu content. Displayed compositional dependences of S_2 and partial entropies correlate with the chemical short-range order (CSRO) changes discussed before. Basically, low CSRO degree on the Al-rich side corresponds to a low negative S_2 value compared to middle Cu composition for which significant degree of CSRO and abundance of icosahedral motifs have been recorded. This is a good demonstration of S_2 function ability to appropriately reflect the local atom arrangements within the nearest neighbour environment, which can be characterized by CSRO or ISRO (icosahedral short-range ordering), in spite of negligence of many-body correlations. Similarly to the impact of CSRO and ISRO on the S_2 function compositional behaviour of Al–Cu liquid alloys, we also notice such confirmation for self-diffusion coefficients' changes. The decrease in both SD coefficients corresponds to respective decreases in S_2^{Al} and S_2^{Cu} entropies. In relation to this, the significant differentiation in SD values and average coordination number between Al and Cu species has a big influence on the trend in excess and partial entropies.

To clarify the effect of diffusion on excess entropy, we inspect the scaled diffusion coefficient (D^*) using Enskog theory which is presented in Fig. 10b as a function of excess entropy S_2 at 1345 K. It has been computed for the all Al–Cu alloys investigated and confronted with the literature data for pure liquid Al [27] and Cu [61] metals. Normalized diffusion D^* computed, using Eq. (9), scales adequately to those displayed by pure liquid Al and Cu atoms, excepting only the liquid binary $Al_{50}Cu_{50}$ system exhibiting a significant coefficient shift. As it can be seen, D^* decreases with increasing ($-S_2$) function and its decrease is compatible with that exhibited in Fig. 10a.

Conclusions

In conclusion, the structure and chemistry of liquid Al–Cu alloys have been studied by means of molecular dynamics, using modified embedded atom model potential and CALPHAD-type modelling based on a quasi-chemical approximation for weakly compound-forming melts (CFM formalism).

The CFM computations provided important knowledge on the interplay between thermodynamics, kinetics and structure over a broad Cu concentration range which allowed to supplement the database of Al–Cu liquid alloy properties. The assumption of Al_2Cu compound dominance within the CFM formalism allowed to accurately reproduce the available experimental data, and consequently explain the experimental structural characterization of two liquid Al–Cu alloys performed by Brillo et al. [35].

Compositional dependence of concentration fluctuation function, $S_{cc}(0)$, displayed significant deviation from regular solution comparable with predictions of the CFM formalism and experimental data. In turn, the nonlinear change of diffusion coefficients (both self and mutual) and viscosity is associated with pronounced chemical short-range ordering (CSRO) increasing with Cu growth confirmed by present molecular dynamics simulations. A significant effect of increasing dense-packing liquid Al–Cu alloys on excess entropy corresponding to an appreciable decrease in partial and total entropies has been found.

To summarize, using the hybrid approach presented herein, we gave a compact and detailed description of the structure, thermodynamics and kinetics of liquid phase, valuable for manufacturing of solid materials based on Al–Cu alloys. The studies presented in this work are the first ones concerning the Al–Cu alloys and the used methodology, which allowed us to find another hard-sphere-like metallic system whose transport properties are strongly affected by packing effects. Thermodynamics-based modelling allowed to quickly cover a broad concentration range compared to molecular dynamics simulations employing semi-empirical interatomic forces fitted to ab initio calculation results. Although the former calculations do not explicitly consider the atomic level, they need to be supported by atomistic computations to gain deeper insight into the physical phenomenology of any studied melt.

Computer Centre CYFRONET AGH using PLGRID Infrastructure.

Author contributions

M.E.T. had the idea for this work and performed all the atomistic simulations and thermodynamics-based modelling, as well as wrote the manuscript. P.W.S. performed Voronoi polyhedral analysis and the geometrical construction of each Voronoi cell, as well as corrected the manuscript. P.A.K. reviewed and corrected the manuscript.

Open Access

This article is distributed under the terms of the Creative Commons Attribution 4.0 International License (http://creativecommons.org/licenses/by/4.0/), which permits unrestricted use, distribution, and reproduction in any medium, provided you give appropriate credit to the original author(s) and the source, provide a link to the Creative Commons license, and indicate if changes were made.

References

[1] Asta M, Morgan D, Hoyt JJ et al (1999) Embedded-atom-method study of structural, thermodynamic, and atomic-transport properties of liquid Ni–Al alloys. Phys Rev B 59:14271–14281. https://doi.org/10.1103/PhysRevB.59.14271

[2] Horbach J, Das SK, Griesche A et al (2007) Self-diffusion and interdiffusion in Al 80 Ni 20 melts: simulation and experiment. Phys Rev B 75:174304. https://doi.org/10.1103/PhysRevB.75.174304

[3] Das SK, Horbach J, Koza MM et al (2005) Influence of chemical short-range order on atomic diffusion in Al–Ni melts. Appl Phys Lett 86:2003–2006. https://doi.org/10.1063/1.1845590

[4] Trybula M, Jakse N, Gasior W, Pasturel A (2014) Structural and physicochemical properties of liquid Al–Zn alloys: a combined study based on molecular dynamics simulations and the quasi-lattice theory. J Chem Phys 141:1–9. https://doi.org/10.1063/1.4903209

[5] Trybula ME (2016) Structure and transport properties of the liquid Al80Cu20 alloy—a molecular dynamics study. Comput Mater Sci 122:341–352. https://doi.org/10.1016/j.commatsci.2016.05.029

[6] Hoyt JJ, Asta M (2002) Atomistic computation of liquid diffusivity, solid-liquid interfacial free energy, and kinetic coefficient in Au and Ag. Phys Rev B 65:214106. https://doi.org/10.1103/PhysRevB.65.214106

[7] Bhatia AB, Singh RN (1984) A quasi-lattice theory for compound forming molten alloys. Phys Chem Liq 13:177–190. https://doi.org/10.1080/00319108408080778

[8] Singh RN (1987) Short-range order and concentration fluctuations in binary molten alloys. Can J Phys 65:309–325. https://doi.org/10.1139/p87-038

[9] Trybula M, Gancarz T, Gasior W, Pasturel A (2014) Bulk and surface properties of liquid Al–Li and Li–Zn alloys. Metall Mater Trans A 45:5517–5530. https://doi.org/10.1007/s11661-014-2524-6

[10] Novakovic R, Muolo ML, Passerone A (2004) Bulk and surface properties of liquid X–Zr (X = Ag, Cu) compound forming alloys. Surf Sci 549:281–293. https://doi.org/10.1016/j.susc.2003.12.006

[11] Murray JL (1985) The aluminium–copper system. Int Met Rev 30:211–234. https://doi.org/10.1179/imtr.1985.30.1.211

[12] Wolverton C, Ozolins V (2001) Entropically favored ordering: the metallurgy of Al_2Cu revisited. Phys Rev Lett 86:5518–5521. https://doi.org/10.1103/PhysRevLett.86.5518

[13] Hu S, Baskes M, Stan M, Chen L (2006) Atomistic calculations of interfacial energies, nucleus shape and size of θ' precipitates in Al–Cu alloys. Acta Mater 54:4699–4707. https://doi.org/10.1016/j.actamat.2006.06.010

[14] Boyd JD, Nicholson RB (1971) The coarsening behaviour of θ'' and θ' precipitates in two Al–Cu alloys. Acta Metall 19:1379–1391. https://doi.org/10.1016/0001-6160(71)90076-9

[15] Shtablavyi I, Mudry S, Mykhaylyuk V, Rybicki J (2008) The structure of Al–Cu and Al–Si eutectic melts. J Non Cryst Solids 354:4469–4474. https://doi.org/10.1016/j.jnoncrysol.2008.06.071

[16] Wang WY, Han JJ, Fang HZ et al (2015) Anomalous structural dynamics in liquid Al 80 Cu 20: an ab initio molecular dynamics study. Acta Mater 97:75–85. https://doi.org/10.1016/j.actamat.2015.07.001

[17] Lee B-JBBJ, Baskes MI (2000) Second nearest-neighbor modified embedded-atom-method potential. Phys Rev B 62:8564–8567. https://doi.org/10.1103/PhysRevB.62.8564

[18] Wang SY, Kramer MJ, Xu M et al (2009) Experimental and ab initio molecular dynamics simulation studies of liquid Al 60 Cu 40 alloy. Phys Rev B 79:144205. https://doi.org/10.1103/PhysRevB.79.144205

[19] Dziedzic J, Winczewski S, Rybicki J (2016) Structure and properties of liquid Al–Cu alloys: empirical potentials

compared. Comput Mater Sci 114:219–232. https://doi.org/10.1016/j.commatsci.2015.12.014

[20] Schick M, Brillo J, Egry I, Hallstedt B (2012) Viscosity of Al–Cu liquid alloys: measurement and thermodynamic description. J Mater Sci 47:8145–8152. https://doi.org/10.1007/s10853-012-6710-x

[21] Dahlborg U, Besser M, Calvo-Dahlborg M et al (2007) Diffusion of Cu in AlCu alloys of different composition by quasielastic neutron scattering. J Non Cryst Solids 353:3295–3299. https://doi.org/10.1016/j.jnoncrysol.2007.05.074

[22] Zhang B, Griesche A, Meyer A (2010) Diffusion in Al–Cu melts studied by time-resolved X-Ray radiography. Phys Rev Lett 104:35902. https://doi.org/10.1103/PhysRevLett.104.035902

[23] Trybula M, Jakse N, Gasior W et al (2015) Thermodynamics and concentration fluctuations of liquid Al–Cu and Al–Zn alloys. Arch Metall Mater 60:649–655. https://doi.org/10.1515/amm-2015-0187

[24] Tanaka T, Gokcen N, Spencer P (1993) Evaluation of interaction parameters in dilute liquid ternary alloys by a solution model based on the free volume theory. Z Metallkd 84:100–105

[25] Trybula M, Gancarz T, Gasior W, Pasturel A (2014) Bulk and surface properties of liquid Al–Li and Li–Zn alloys. Metall Mater Trans A Phys Metall Mater Sci. https://doi.org/10.1007/s11661-014-2524-6

[26] Novakovic R, Tanaka T, Muolo ML et al (2005) Bulk and surface properties of liquid Ag–X (X = Ti, Hf) compound forming alloys. Surf Sci 591:56–69. https://doi.org/10.1016/j.susc.2005.06.022

[27] Dzugutov M (1996) A universal scaling law for atomic diffusion in condensed matter. Nature 381:137–139. https://doi.org/10.1038/35079655

[28] Chapman C, Cowling TG (1970) The mathematical theory of non-uniform gases. Cambridge University Press, London

[29] Bhatia AB, Singh RN (1982) Thermodynamic properties of compound forming molten alloys in a weak interaction approximation. Phys Chem Liq 11:343–351. https://doi.org/10.1080/00319108208080755

[30] Prasad LC, Jha RK (2005) Surface tension and viscosity of Sn-based binary liquid alloys. Phys status solidi 202:2709–2719. https://doi.org/10.1002/pssa.200520080

[31] Prasad L, Singh R (1991) Surface segregation and concentration fluctuations at the liquid-vapor interface of molten Cu–Ni alloys. Phys Rev B 44:13768–13771. https://doi.org/10.1103/PhysRevB.44.13768

[32] Bhatia A, Hargrove W, Thornton D (1974) Concentration fluctuations and partial structure factors of compound-forming binary molten alloys. Phys Rev B 9:435–444. https://doi.org/10.1103/PhysRevB.9.435

[33] Warren BE (1969) X-ray diffraction. Addison-Wesley, Reading

[34] Bhatia AB, Singh RN (1982) Short range order and concentration fluctuations in regular and compound forming molten alloys. Phys Chem Liq 11:285–313. https://doi.org/10.1080/00319108208080752

[35] Brillo J, Bytchkov A, Egry I et al (2006) Local structure in liquid binary Al–Cu and Al–Ni alloys. J Non Cryst Solids 352:4008–4012. https://doi.org/10.1016/j.jnoncrysol.2006.08.011

[36] Plimpton SJ (1995) Fast parallel algorithms for short-range molecular dynamics. J Comput Phys 117:1–19. https://doi.org/10.1006/jcph.1995.1039

[37] Brillo J, Egry I, Ho I (2006) Density and thermal expansion of liquid Ag–Cu and Ag–Au Alloys. 27:494–506. https://doi.org/10.1007/s10765-005-0011-4

[38] Rycroft C (2009) Voro ++: a three-dimensional Voronoi cell library in C ++. Chaos 19:41111. https://doi.org/10.1063/1.3215722

[39] Darken L (1948) Diffusion, mobility and their interrelation through free energy in binary metallic systems. Trans Met Soc Aime 175:184

[40] Jacucci G, McDonald I (1980) Collective excitations in a liquid alloy. J Phys F: Met Phys 10:L15–L19. https://doi.org/10.1088/0305-4608/10/1/003

[41] Redlich O, Kister AT (1948) Algebraic representation of thermodynamic properties and the classification of solutions. Ind Eng Chem 40:345–348. https://doi.org/10.1021/ie50458a036

[42] Harris KR (2009) The fractional Stokes–Einstein equation: application to Lennard–Jones, molecular, and ionic liquids. J Chem Phys 131:54503. https://doi.org/10.1063/1.3183951

[43] Hoover WG, Evans DJ, Hickman RB et al (1980) Lennard–Jones triple-point bulk and shear viscosities. Green–Kubo theory, Hamiltonian mechanics, and nonequilibrium molecular dynamics. Phys Rev A 22:1690–1697. https://doi.org/10.1103/PhysRevA.22.1690

[44] Witusiewicz VT, Hecht U, Fries SG, Rex S (2004) The Ag–Al–Cu system. J Alloys Compd 385:133–143. https://doi.org/10.1016/j.jallcom.2004.04.126

[45] Kargl F, Weis H, Unruh T, Meyer A (2012) Self diffusion in liquid aluminium. J Phys: Conf Ser 340:12077. https://doi.org/10.1088/1742-6596/340/1/012077

[46] Meyer A (2010) Self-diffusion in liquid copper as seen by quasielastic neutron scattering. Phys Rev B Condens Matter Mater Phys 81:2009–2011. https://doi.org/10.1103/PhysRevB.81.012102

[47] Bhatia A, Hargrove W (1974) Concentration fluctuations and thermodynamic properties of some compound forming binary molten systems. Phys Rev B 10:3186–3196. https://doi.org/10.1103/PhysRevB.10.3186

[48] Brillo J, Chathoth SM, Koza MM, Meyer A (2008) Liquid Al$_{80}$Cu$_{20}$: atomic diffusion and viscosity. Appl Phys Lett 93:121905. https://doi.org/10.1063/1.2977863

[49] Ojwang' JGO, Van Santen R, Kramer GJ, et al (2008) Predictions of melting, crystallization, and local atomic arrangements of aluminum clusters using a reactive force field. J Chem Phys. https://doi.org/10.1063/1.3050278

[50] Pasturel A, Jakse N (2015) On the role of entropy in determining transport properties in metallic melts. J Phys Condens Matter 27:325104. https://doi.org/10.1088/0953-8984/27/32/325104

[51] Saw CK, Schwarz RB (1988) Chemical short-range order parameter in dense random-packed models. J Less Common Met 140:385–393. https://doi.org/10.1016/0022-5088(88)90399-2

[52] Das SK, Horbach J, Koza MM et al (2005) Influence of chemical short-range order on atomic diffusion in Al–Ni melts. Appl Phys Lett 86:11918. https://doi.org/10.1063/1.1845590

[53] Protopapas P, Andersen HC, Parlee NAD (1973) Theory of transport in liquid metals. I. Calculation of self-diffusion coefficients. J Chem Phys 59:15. https://doi.org/10.1063/1.1679784

[54] Foffi G, Götze W, Sciortino F et al (2003) Mixing effects for the structural relaxation in binary hard-sphere liquids. Phys Rev Lett 91:85701. https://doi.org/10.1103/PhysRevLett.91.085701

[55] Trybula M (2015) Thermodynamic, structural and thermophysical properties of liquid Al–Li–Zn alloys, Ph.D. Thesis, 2015 IMMS PAS

[56] Stukowski A (2012) Structure identification methods for atomistic simulations of crystalline materials. Model Simul Mater Sci Eng 20:45021–1–45021–18. https://doi.org/10.1088/0965-0393/20/4/045021

[57] Yu HB, Samwer K, Wang WH, Bai HY (2013) Chemical influence on β-relaxations and the formation of molecule-like metallic glasses. Nat Commun 4:1–6. https://doi.org/10.1038/ncomms3204

[58] Yu HB, Samwer K, Wu Y, Wang WH (2012) Correlation between β relaxation and self-diffusion of the smallest constituting atoms in metallic glasses. Phys Rev Lett 109:1–5. https://doi.org/10.1103/PhysRevLett.109.095508

[59] Yu H, Wang W, Samwer K (2013) The β relaxation in metallic glasses: an overview. Mater Today 16:6–20. https://doi.org/10.1016/j.mattod.2013.05.002

[60] Angell CA (1995) Formation of glasses from liquids and biopolymers. Science 267:1924–1935. https://doi.org/10.1126/science.267.5206.1924

[61] Hoyt J, Asta M, Sadigh B (2000) Test of the universal scaling law for the diffusion coefficient in liquid metals. Phys Rev Lett 85:594–597. https://doi.org/10.1103/PhysRevLett.85.594

[62] Angell C (1991) Relaxation in liquids, polymers and plastic crystals—strong/fragile patterns and problems. J Non Cryst Solids 131–133:13–31. https://doi.org/10.1016/0022-3093(91)90266-9

[63] Debenedetti P, Stillinger F (2001) Supercooled liquids and the glass transition. Nature 410:259–267. https://doi.org/10.1038/35065704

[64] Eskin D, Du Q, Ruvalcaba D, Katgerman L (2005) Experimental study of structure formation in binary Al–Cu alloys at different cooling rates. Mater Sci Eng, A 405:1–10. https://doi.org/10.1016/j.msea.2005.05.105

[65] Dong HB, Lee PD (2005) Simulation of the columnar-to-equiaxed transition in directionally solidified Al–Cu alloys. Acta Mater 53:659–668. https://doi.org/10.1016/j.actamat.2004.10.019

[66] Gill SC, Kurz W (1993) Rapidly solidified AlCu alloys-I. experimental determination of the microstructure selection map. Acta Metall Mater 41:3563–3573. https://doi.org/10.1016/0956-7151(93)90237-M